Deep subnanosecond spin torque switching in magnetic tunnel junctions with combined in-plane and perpendicular polarizers

G. E. Rowlands,[1] T. Rahman,[2] J. A. Katine,[3] J. Langer,[4] A. Lyle,[2] H. Zhao,[2] J. G. Alzate,[5] A. A. Kovalev,[6] Y. Tserkovnyak,[6] Z. M. Zeng,[6] H. W. Jiang,[6] K. Galatsis,[5] Y. M. Huai,[7] P. Khalili Amiri,[5] K. L. Wang,[5] I. N. Krivorotov,[1,a)] and J.-P. Wang[2,b)]
[1]*Physics and Astronomy, University of California, Irvine, California 92697, USA*
[2]*Electrical and Computer Engineering, University of Minnesota, Minneapolis, Minnesota 55455, USA*
[3]*Hitachi Global Storage Technologies, 3403 Yerba Buena Road, San Jose, California 95135, USA*
[4]*Singulus Technologies, 63796 Kahl am Main, Germany*
[5]*Electrical Engineering, University of California, Los Angeles, California 90095, USA*
[6]*Physics and Astronomy, University of California, Los Angeles, California 90095, USA*
[7]*Avalanche Technology, 48371 Fremont Blvd., Suite 101, Fremont, California 94538, USA*

(Received 2 February 2011; accepted 22 February 2011; published online 10 March 2011)

We show that adding a perpendicular polarizer to a conventional spin torque memory element with an in-plane free layer and an in-plane polarizer can significantly increase the write speed and decrease the write energy of the element. We demonstrate the operation of such spin torque memory elements with write energies of 0.4 pJ and write times of 0.12 ns. © *2011 American Institute of Physics*. [doi:10.1063/1.3565162]

Since the initial prediction[1,2] and experimental demonstration[3] of magnetization reversal by spin transfer torque (STT), there has been continuous progress toward the development of nonvolatile magnetic random access memory based on STT switching (STT-RAM) in nanoscale magnetic tunnel junctions (MTJs).[4–11] In the most common STT-RAM configuration shown in Fig. 1(a), the magnetic moments of the free layer and the pinned polarizing layer of an MTJ lie collinear to one another in the plane of the junction. In this configuration (in-plane STT-RAM or IST-RAM), STT is small during the initial stages of the free layer's magnetic moment reversal, resulting in a relatively long nanosecond-scale switching time.[12,13] Switching can be greatly accelerated in an alternative STT-RAM configuration, in which a second polarizer with magnetic moment perpendicular to the MTJ plane is added to the magnetic multilayer (orthogonal STT-RAM or OST-RAM).[14] The initial STT from the perpendicular polarizer is large and has been predicted to induce ultrafast precessional switching of the free layer's magnetization on a time scale of 100 ps.[14] Such ultrafast switching induced by a perpendicular polarizer was recently demonstrated in both giant magnetoresistance (GMR) junctions[15–17] and hybrid MTJ/GMR structures.[18]

In this letter, we report ultrafast switching of magnetization in dual-MTJ OST-RAM structures shown in Fig. 1(b). We present a direct comparison of STT switching in IST-RAM and OST-RAM devices with nearly identical dimensions and multilayer compositions except for the presence of the perpendicular polarizer in the OST-RAM structure. Our work gives an example of the improvement in write speed and energy that can be offered by OST-RAM devices over IST-RAM devices.

The OST-RAM devices studied in this letter are 180×70 nm^2 elliptical nanopillars shown in Fig. 1(b) patterned from the following multilayer: (bottom lead)/(in-plane polarizer)/(barrier)/(free layer)/(barrier)/(perpendicular polarizer)/(cap). In these devices, (in-plane polarizer) $\equiv Pt_{37}Mn_{63}(20)/Co_{70}Fe_{30}(2.5)/Ru(0.85)/Co_{40}Fe_{40}B_{20}(2.4)$, (perpendicular polarizer) $\equiv Co_{60}Fe_{20}B_{20}(0.75)/[Co(0.3)/Pd(1.0)]_{10}$, (barrier) $\equiv$ MgO(0.82), and (free layer) $\equiv Co_{60}Fe_{20}B_{20}(2.0)$ with the layer thicknesses given in nanometers. The reference IST-RAM devices are 160×65 nm^2 elliptical nanopillars patterned from (bottom lead)/(in-plane polarizer)/(barrier)/(free layer)/(cap), where (in-plane polarizer) $\equiv Pt_{37}Mn_{63}(15)/Co_{70}Fe_{30}(2.5)/Ru(0.85)/Co_{40}Fe_{40}B_{20}(2.4)$, (barrier) $\equiv$ MgO(0.82), and (free layer) $\equiv Co_{60}Fe_{20}B_{20}(1.8)$. The multilayers were grown by magnetron sputtering in a Singulus TIMARIS system and annealed at 300 °C for 2 h in a 1 T in-plane field.

All magnetic layers are patterned into elliptical nanopillars with the long axis parallel to the annealing field direction. The perpendicular magnetic anisotropy of the $[Co(0.3)/Pd(1.0)]_{10}$ superlattice forces the magnetic moment

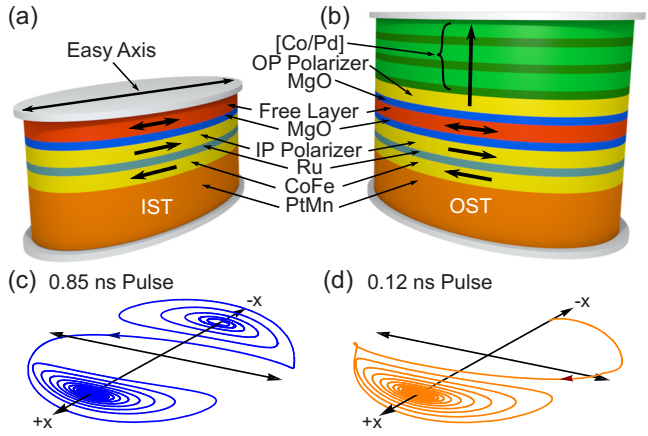

FIG. 1. (Color online) (a) Schematic of the IST-RAM device consisting of a pinned in-plane synthetic antiferromagnetic polarizer and a CoFeB free layer. (b) OST-RAM device made by adding a perpendicular polarizer to the IST-RAM device. [(c) and (d)] Simulated macrospin trajectories of magnetizations starting near the $-\hat{x}$ direction in response to 2.4×10^7 A/cm^2 square pulses in (c) IST-RAM and (d) OST-RAM.

a)Electronic mail: ikrivoro@uci.edu.
b)Electronic mail: jpwang@umn.edu.

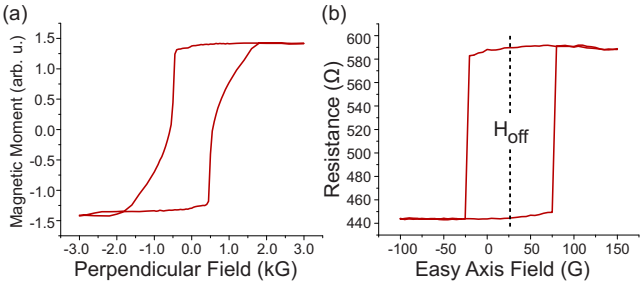

FIG. 2. (Color online) (a) VSM measurement of an unpatterned OST-RAM multilayer for a magnetic field applied perpendicular to the plane. (b) Resistance of an OST-RAM device versus in-plane easy-axis magnetic field.

of the top polarizer to point orthogonal to the plane of the sample. The 0.75 nm thick $Co_{60}Fe_{20}B_{20}$ layer of the perpendicular polarizer is used to enhance the magnitude of STT applied to the free layer. We use vibrating sample magnetometry (VSM) to verify the presence of perpendicular magnetic anisotropy in the additional polarizer. Figure 2(a) shows VSM measurements for a magnetic field applied perpendicular to the plane of an unpatterned multilayer. The effectiveness of the $[Co(0.3)/Pd(1.0)]_{10}$ superlattice as a perpendicular polarizer is demonstrated by a nearly 100% remanence of the polarizer's magnetization. Figure 2(b) shows resistance versus magnetic field applied in the plane of an OST-RAM device along the long axis of the ellipse. The observed magnetoresistance is due to switching of the free layer's magnetic moment between parallel and antiparallel configurations with the in-plane polarizer.

The differences in the reversal modes expected for the IST-RAM and OST-RAM devices are illustrated in Figs. 1(c) and 1(d), wherein magnetization switching trajectories are shown for the two types of memory as calculated in the macrospin approximation by numerical integration of the Landau–Lifshitz–Gilbert equation with Slonczewski spin torque term.[19] In these simulations we use material parameters appropriate for our devices: saturation magnetization of the free layer $M_s=1200$ emu/cm^3, current spin polarization $P=0.5$ for both the in-plane and the perpendicular polarizers, Gilbert damping parameter $\alpha=0.015$, and diagonal demagnetizing tensor ($N_{xx}=0.943$, $N_{yy}=0.045$, and $N_{zz}=0.012$).[20] The initial in-plane angle of the free layer's magnetic moment from the easy axis, 4.8°, is calculated as the root-mean-square angle due to thermal fluctuation of magnetization at room temperature. The IST-RAM switching trajectory in Fig. 1(c) shows several preswitching precession cycles and thus the switching process is relatively slow. The IST-RAM switching is slow due to the small initial magnitude of STT, which is proportional to sine of the angle between the magnetic moments of the free and the polarizer layers.[1] For OST-RAM, STT from the perpendicular polarizer is large and it immediately pushes the free layer magnetic moment out of the sample plane. As a result, the free layer magnetic moment rapidly reverses via one half of a precession cycle around the out-of-plane demagnetizing field as shown in Fig. 1(d).

We test the predicted differences in the switching behavior of IST-RAM and OST-RAM devices by measuring the probability of reversal of the free layer in response to voltage pulses of varying magnitude and duration. These switching studies are performed at the center of the free layer's hysteresis loop, H_{off}, as shown in Fig. 2(b). We apply voltage

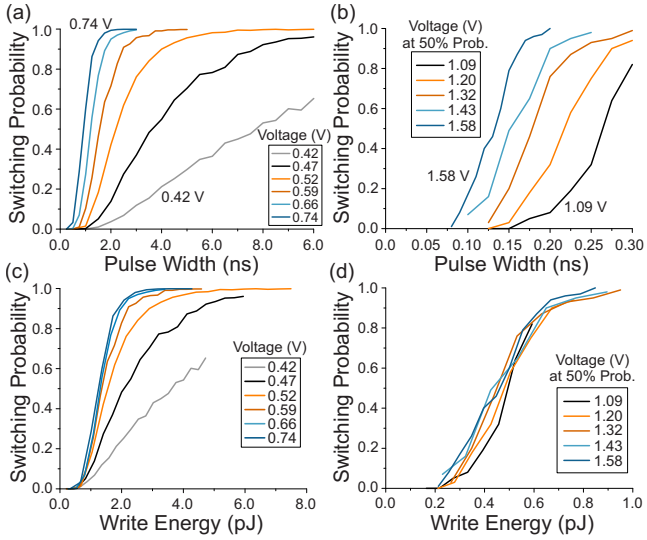

FIG. 3. (Color online) Switching probability as a function of the applied voltage pulse duration and magnitude for (a) IST-RAM and (b) OST-RAM devices. Voltage labels for OST-RAM data are the values at 50% switching probability. Switching probability as a function of energy delivered to (c) IST-RAM and (d) OST-RAM devices.

pulses and measure the final device resistance using a bias tee. Before each voltage pulse, the device is prepared in the low resistance (parallel) state and the probability of switching into the high resistance (antiparallel) state is measured. The polarity of the applied voltage pulses corresponds to electron flowing from the free layer to the in-plane polarizer.

Switching probability for an IST-RAM device is shown in Fig. 3(a) as a function of the applied voltage pulse magnitude and duration. These data illustrate that the pulse width required to achieve 50% switching probability, t_{50}, decreases with increasing pulse amplitude but remains long: 0.92 ns even at the maximum pulse amplitude of 0.74 V. Figure 3(b) shows the switching probability as a function of the pulse duration for the OST-RAM device shown in Fig. 2(b). A large reduction in switching time in the OST-RAM devices is apparent, with the shortest observed value of 0.12 ns at the pulse amplitude of 1.58 V.[21] This fast switching time is in agreement with theoretical predictions for OST-RAM devices[14] and the simulation results shown in Fig. 1(d). For both IST-RAM and OST-RAM devices, the maximum switching voltage is limited by the irreversible breakdown of ultrathin MgO tunnel barriers. Since our OST-RAM is composed of two barriers in series, the maximum voltage that can be applied to the structure without breakdown (~2 V) is twice that for IST-RAM (~1 V). When operating near the maximum safe pulse amplitudes, the data in Fig. 3 demonstrate a factor of eight reduction in the switching time for OST-RAM when compared to IST-RAM devices. We do not observe oscillations of the switching probability with pulse duration that may be expected for precessional switching of OST-RAM.[14] This observation is in agreement with the recent measurements for hybrid MTJ/GMR OST-RAM devices.[18] We attribute the absence of such oscillations to the influence of STT generated by the in-plane polarizer.

Figure 4(a) shows the dependence of the switching voltage amplitude at 50% switching probability, V_{50}, on the write pulse duration, t_{50}, for both IST-RAM and OST-RAM devices. This figure clearly illustrates that the OST-RAM devices operate on a much faster time scale than their IST-

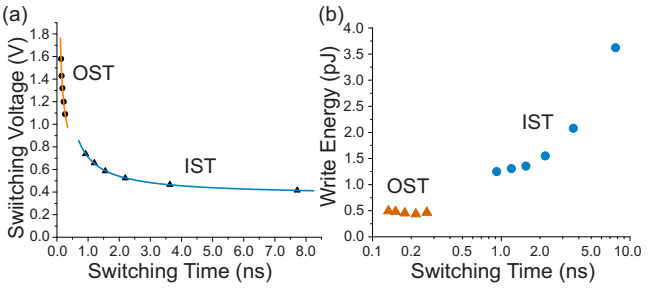

FIG. 4. (Color online) (a) Switching voltage for IST-RAM and OST-RAM devices plotted as a function of pulse width at 50% switching probability, t_{50}. Solid lines are best fits described in the text. (b) Energy per write at 50% switching probability plotted as a function of switching time, t_{50}.

RAM counterparts. The data in Fig. 4(a) are well fit by $V_{50}=V_c(1+\tau_0/t_{50})$ for both IST-RAM and OST-RAM with V_c and τ_0 giving the critical write voltage and characteristic switching time.[12] The best fit gives $V_c=0.37$ V and $\tau_0=0.91$ ns for the IST-RAM device and $V_c=0.61$ V and $\tau_0=0.21$ ns for the OST-RAM devices.

To quantify the write energy reduction in OST-RAM, we plot the switching probability as a function of energy dissipated during the write process in Figs. 3(c) and 3(d). The write energy is calculated as $E_w=\int V_a^2(t)dt(1+\Gamma)^2/R_P$, where $V_a(t)$ is the actual voltage pulse shape measured by replacing the sample with a 20 GHz sampling oscilloscope, Γ is the reflection coefficient at the sample, and R_P is the sample resistance in the initial parallel state. Figure 4(b) shows the write energy required to achieve 50% switching probability as a function of write pulse width, t_{50}, for both IST-RAM and OST-RAM devices. The minimum write energy for OST-RAM devices is 0.4 pJ, which is a significant reduction over the IST-RAM device, for which the minimum energy per write is 1.25 pJ. We note that further reduction in the write energy can be achieved by replacing the MTJ formed by the perpendicular polarizer and the free layer by a GMR junction.[18] If such a replacement were carried out without a decrease in the magnitude of STT from the perpendicular polarizer, the write voltage could be reduced by a factor of two and the write energy by a factor of four. Therefore, write energy as low as 0.1 pJ can be expected for OST-RAM devices.

In conclusion, we have shown that adding a perpendicular polarizer to a standard IST-RAM device can significantly reduce the write time and the write energy. For a typical multilayer structure and STT-RAM cell dimensions, we observe an eightfold write time reduction and a threefold write energy reduction. Our results suggest that STT-RAM devices with write times as low as 0.1 ns and write energies as low as 0.1 pJ are feasible.

This work was supported by DARPA Grant No. HR0011-09-C-0114, by NSF Grant Nos. DMR-0748810 and No. ECCS-0701458, and by Nanoelectronics Research Initiative through the Western Institute of Nanoelectronics.

[1] J. C. Slonczewski, J. Magn. Magn. Mater. **159**, L1 (1996).
[2] L. Berger, Phys. Rev. B **54**, 9353 (1996).
[3] J. A. Katine, F. J. Albert, R. A. Buhrman, E. B. Myers, and D. C. Ralph, Phys. Rev. Lett. **84**, 3149 (2000).
[4] Y. Huai, F. Albert, P. Nguyen, M. Pakala, and T. Valet, Appl. Phys. Lett. **84**, 3118 (2004).
[5] G. D. Fuchs, N. C. Emley, I. N. Krivorotov, P. M. Braganca, E. M. Ryan, S. I. Kiselev, J. C. Sankey, D. C. Ralph, R. A. Buhrman, and J. A. Katine, Appl. Phys. Lett. **85**, 1205 (2004).
[6] H. Kubota, A. Fukushima, Y. Ootani, S. Yuasa, K. Ando, H. Maehara, K. Tsunekawa, D. D. Djayaprawira, N. Watanabe, and Y. Suzuki, Jpn. J. Appl. Phys., Part 2 **44**, L1237 (2005).
[7] J. Hayakawa, S. Ikeda, Y. M. Lee, R. Sasaki, T. Meguro, F. Matsukura, H. Takahashi, and H. Ohno, Jpn. J. Appl. Phys., Part 2 **44**, L1267 (2005).
[8] H. Meng and J. P. Wang, Appl. Phys. Lett. **88**, 172506 (2006).
[9] P. M. Braganca, J. A. Katine, N. C. Emley, D. Mauri, J. R. Childress, P. M. Rice, E. Delenia, D. C. Ralph, and R. A. Buhrman, IEEE Trans. Nanotechnol. **8**, 190 (2009).
[10] J. Z. Sun, M. C. Gaidis, E. J. O'Sullivan, E. A. Joseph, G. Hu, D. W. Abraham, J. J. Nowak, P. L. Trouilloud, Y. Lu, S. L. Brown, D. C. Worledge, and W. J. Gallagher, Appl. Phys. Lett. **95**, 083506 (2009).
[11] K. Yakushiji, K. Noma, T. Saruya, H. Kubota, A. Fukushima, T. Nagahama, S. Yuasa, and K. Ando, Appl. Phys. Express **3**, 053003 (2010).
[12] J. Z. Sun, Phys. Rev. B **62**, 570 (2000).
[13] D. E. Nikonov, G. I. Bourianoff, G. Rowlands, and I. N. Krivorotov, J. Appl. Phys. **107**, 113910 (2010).
[14] A. D. Kent, B. Ozyilmaz, and E. del Barco, Appl. Phys. Lett. **84**, 3897 (2004).
[15] O. J. Lee, V. S. Pribiag, P. M. Braganca, P. G. Gowtham, D. C. Ralph, and R. A. Buhrman, Appl. Phys. Lett. **95**, 012506 (2009).
[16] C. Papusoi, B. Delaët, B. Rodmacq, D. Houssameddine, J.-P. Michel, U. Ebels, R. C. Sousa, L. Buda-Prejbeanu, and B. Dieny, Appl. Phys. Lett. **95**, 072506 (2009).
[17] J. M. L. Beaujour, D. B. Bedau, H. Liu, M. R. Rogosky, and A. D. Kent, *Spintronics II* (SPIE, San Diego, 2009), Vol. 7398, p. 7398D-11.
[18] H. Liu, D. Bedau, D. Backes, J. A. Katine, J. Langer, and A. D. Kent, Appl. Phys. Lett. **97**, 242510 (2010).
[19] J. C. Slonczewski and J. Z. Sun, J. Magn. Magn. Mater. **310**, 169 (2007).
[20] M. Beleggia, M. De Graef, Y. T. Millev, D. A. Goode, and G. Rowlands, J. Phys. D: Appl. Phys. **38**, 3333 (2005).
[21] The values of the voltage pulse amplitudes given in Figs. 3(b) and 3(d) are, as a consequence of equipment constraints, only valid at a particular pulse duration (the pulse duration at 50% switching probability). When pulse widths become comparable to the rise and fall times of the pulse generator, 65 ps and 85 ps respectively, the pulses begin to suffer some attenuation that increases with decreasing pulse width. At a 120 ps pulse width, for example, a 2.09 V nominal pulse amplitude is reduced to 1.58 V. The attenuation becomes negligible for pulses longer than ~300 ps.